

Impact of non-Maxwellian electron velocity distribution functions on inferred plasma parameters in collective Thomson scattering

A. L. Milder,^{1,2} S. T. Ivancic,¹ J. P. Palastro,¹ and D. H. Froula^{1,2}

¹*Laboratory for Laser Energetics, 250 E. River Rd, Rochester, NY 14623, USA*

²*Department of Physics and Astronomy, University of Rochester, Rochester, NY 14623, USA*

(Dated: 30 January 2019)

Optical collective Thomson scattering provides precise density and temperature measurements in numerous plasma-physics experiments. The accuracy of such measurements depends on the core assumption that the underlying electron distribution functions in under-dense laser-produced plasmas are Maxwellian. A statistically based, quantitative analysis of the errors in the measured electron density and temperature is presented when synthetic data calculated using a non-Maxwellian electron distribution function is fit assuming a Maxwellian electron distribution. Such analysis can lead to errors of up to 50% in temperature and 30% in density, in the specific case of super-Gaussian distributions characteristic of inverse bremsstrahlung heating. Including the proper family of non-Maxwellian electron distribution functions, as a fitting parameter, in Thomson-scattering analysis removes the model-dependent errors in the inferred parameters at minimal cost to the statistical uncertainty.

I. INTRODUCTION

Optical Thomson scattering is a powerful diagnostic that is widely used to measure plasma conditions in laser-produced plasmas.^{1–10} As large multibeam facilities are constructed to achieve inertial confinement fusion around the world,^{11–13} accurate measurements of plasma conditions are becoming increasingly important for understanding the importance of missing physics in the large hydrodynamic simulations. Local and time-resolved measurements of Thomson-scattered spectra have provided valuable insight into a range of studies, including laser-plasma instabilities,^{2–6} thermal transport,^{7,8} and more generally inertial confinement fusion.^{9,10}

The high density present in laser-produced plasmas results in scattering optical light from collective plasma-wave fluctuations. The scattering from low-frequency fluctuations generates ion-acoustic spectral features, while scattering from high-frequency fluctuations generates electron-plasma wave spectral features. Early collective scattering measurements from high-frequency fluctuations¹⁴ used the theory developed two decades earlier by Salpeter¹⁵ to associate the wavelength of spectral peaks with density, through the Bohm-Gross dispersion relation, and the width of spectral peaks to temperature, through Landau damping, but the small scattering cross section for Thomson scattering has resulted in relatively few experiments where electron temperature and density were measured from the electron plasma wave features.^{9,16–19} Recent experiments have used the full Thomson-scattered spectrum to extract plasma conditions, but these studies have been limited to assuming Maxwellian distribution functions. However, variation in the shape of the distribution functions can lead to significant changes to the Thomson-scattering spectrum (Fig. 1).^{19,20}

In this paper, we investigate the sensitivity of electron temperature and density inferred from collective

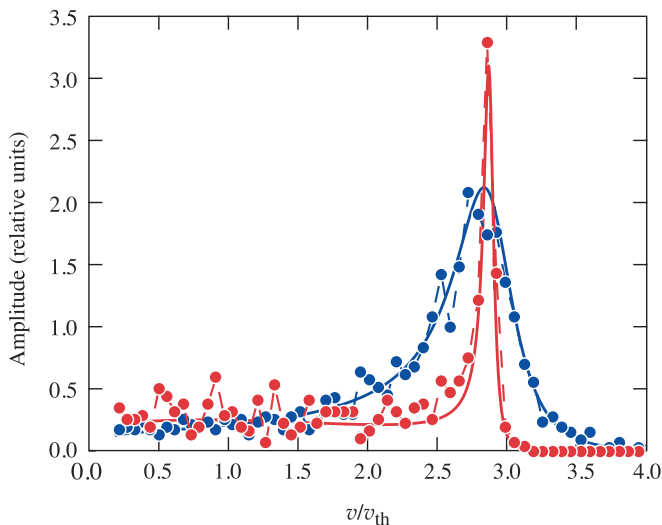
Thomson scattering to non-Maxwellian electron distribution functions, specifically super-Gaussian distribution functions. Analyzing synthetic electron plasma wave Thomson-scattering spectra, under the false assumption that the electron distribution function is Maxwellian, can lead to gross errors in the inferred electron density and temperature. When the true distribution function is super-Gaussian, the errors can be up to 50% in temperature and 30% in density. These errors stem from changes in the shape of the scattered spectra (Fig. 1), and can be removed by including the correct shape of the electron distribution function in the analysis. Other changes to the shape of the electron distribution function can result in errors in the inferred parameters, as in the case of heat flux.⁷

In Section II, the method for producing synthetic data scattered from a non-Maxwellian plasma is presented. The errors incurred by fitting non-Maxwellian data when assuming the spectrum results from a Maxwellian plasma is discussed in Section III. Section IV describes the process for eliminating these errors by including non-Maxwellian electron distribution functions in the analysis process. The paper is summarized in Section V.

II. METHODOLOGY

Figure 1 shows two synthetic spectra generated with the same plasma conditions, but assuming Maxwellian ($m = 2$) and non-Maxwellian ($m = 5$) electron distribution functions. To determine the plasma conditions, Thomson-scattering spectra are typically fit using the collisionless spectral density function¹,

$$S(\mathbf{k}, \omega) = \frac{2\pi}{k} \left| 1 - \frac{\chi_e}{\epsilon} \right|^2 f_e \left(\frac{\omega}{k} \right) + \frac{2\pi Z}{k} \left| \frac{\chi_e}{\epsilon} \right|^2 f_i \left(\frac{\omega}{k} \right) \quad (1)$$



E28024J2

FIG. 1: Theoretical spectrum for Thomson scattering from a Maxwellian plasma (blue) and a non-Maxwellian plasma with super-Gaussian order 5 (red). The circles represent synthetic data generated from the theoretical curves.

where

$$\chi_{e,i}(\mathbf{k}, \omega) = \int_{-\infty}^{\infty} d\mathbf{v} \frac{4\pi e_{e,i}^2 n_{e,i}}{m_{e,i} k^2} \frac{\mathbf{k} \cdot \partial f_{e,i} / \partial \mathbf{v}}{\omega - \mathbf{k} \cdot \mathbf{v}} \quad (2)$$

and

$$\epsilon = 1 + \chi_e(\mathbf{k}, \omega) + \chi_i(\mathbf{k}, \omega). \quad (3)$$

Here, Z is the average ionization state and $n_{e,i}$ are the electron and ion densities. The wave vector ($\mathbf{k} = \mathbf{k}_0 - \mathbf{k}_s$) and frequency ($\omega = \omega_0 - \omega_s$) of the probed fluctuations are given by the Thomson-scattering probe laser (ω_0, \mathbf{k}_0) and the resulting scattered light (ω_s, \mathbf{k}_s). To generate the Thomson-scattering spectra for this study, electron distribution functions following the form proposed in Refs. 21–23, and experimentally observed in Ref. 24, were used. These super-Gaussian distribution functions are the result of inverse bremsstrahlung heating. During inverse bremsstrahlung heating the slower electrons are preferentially heated, depleting the number of slow electrons and increasing the number of electrons near the thermal velocity.

$$F_e(\mathbf{x}) = C_m \exp\{-(x/x_0)^m\} \quad (4)$$

$$x_0 = \sqrt{\frac{3\Gamma(3/m)}{\Gamma(5/m)}} \quad (5)$$

Where $x = v/v_{th}$ is the electron velocity normalized to the thermal velocity, and m is a continuously varying

($2 < m < 5$) parameter called the super-Gaussian order. C_m is a normalization factor such that F_e volume integrates to unity,

$$C_m = \frac{1}{(2\pi)^{3/2} v_{th}^3} 3\sqrt{\frac{\pi}{2}} \frac{m\Gamma(5/m)^{3/2}}{[3\Gamma(3/m)]^{5/2}}. \quad (6)$$

This normalization preserves the standard definitions of temperature and density in relation to the velocity moments of the distribution function. To evaluate Eq. (1), F_e is projected along the Thomson-scattering wave vector (\mathbf{k} with unit vector \hat{k}),

$$f_e(x) = \int d\mathbf{x} F_e(\mathbf{x}) \delta(\hat{k} \cdot \mathbf{x} - \omega/kv_{th}). \quad (7)$$

To generate the synthetic spectra (Fig. 1), the calculated spectra was down-sampled to match the spectral resolution (2 nm/resolution unit) of a typical Thomson-scattering diagnostic²⁵ and scaled so the final signal-to-noise ratio would be 10 at the peak of the signal. Poisson noise was added to each resolution unit by drawing a random number from a Poisson distribution whose mean was the original number of counts in that bin. Adding noise in this way approximates a realistic diagnostic signal; any further sources of noise or reduction in the signal-to-noise ratio would increase the uncertainty in the analysis, but have no effect on the errors found in this paper.

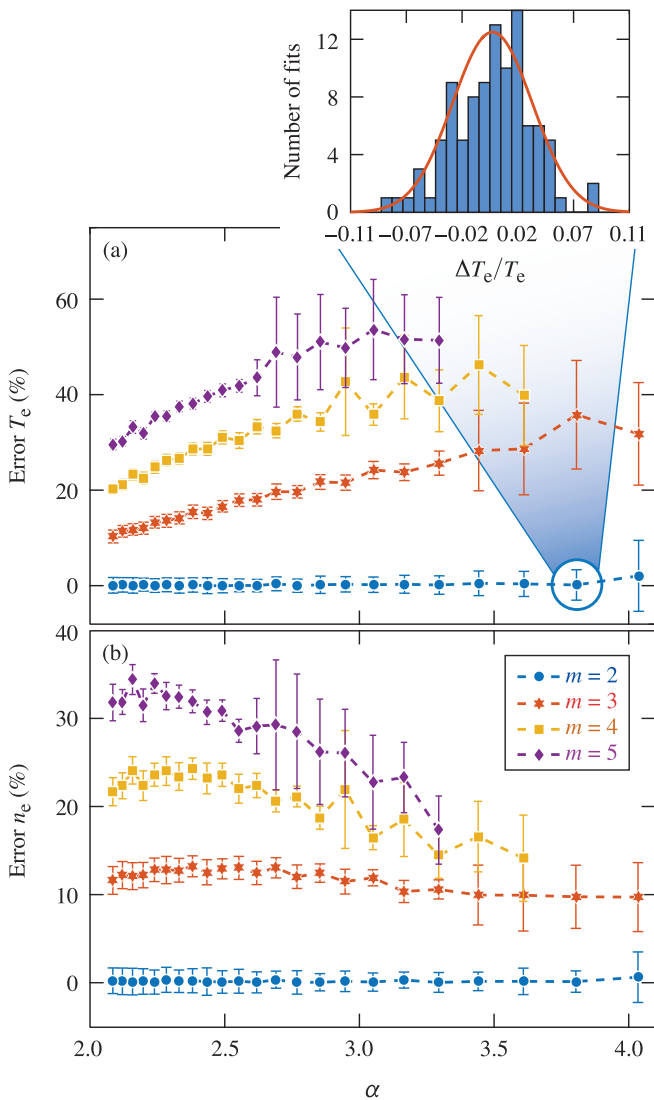
As is traditionally done to analyze experimental data,^{1,9,16,17} the synthetic data was fit with a spectrum calculated from Eq. (1) while assuming a Maxwellian electron distribution function ($m = 2$). A 2-D least-squares statistical analysis was performed across the simulated spectrum by varying the electron density (n_e) and temperature (T_e). The sum of the squared deviation from the data was used as a fit metric (Δ^2), thereby treating each point equally. This fit metric was minimized using an interior-point algorithm.²⁶

To determine the uncertainty in the fit parameters, each synthetic data set was fit multiple times and each fit was performed with a new realization of the Poisson noise and a new random initial guess. The distribution of the fit parameters, from the set of fits, was used to determine the uncertainty in the fit parameters (Fig 2 inset). The average value of the parameter and one standard deviation are reported as the inferred parameter and its uncertainty.

III. MAXWELLIAN ANALYSIS

A. Pure super-Gaussian

Figure 2 shows that the inferred temperature and density can differ from the actual values by 50% and 30%, respectively. As expected, there is no error when fitting Maxwellian data with Maxwellian theory, but this provides a benchmark for the analysis and quantifies the



E28025J2

FIG. 2: Percent error in (a) temperature and (b) density as a function of the normalized phase velocity (α) when the fit model assumes a Maxwellian electron distribution function and the true electron distribution function is super-Gaussian. The absolute difference between the inferred and actual parameter divided by the actual parameter (percent error) is calculated for a range of phase velocities. The values for 4 different super-Gaussian orders are plotted in different colors with error bars that represent the standard deviation of 100 fits.

general uncertainties in the fitting process. For non-Maxwellian plasmas ($m > 2$), the percent error in temperature increases as a function of the super-Gaussian order and normalized phase velocity ($\alpha = v_\phi/v_{th}$). The statistical uncertainty in the inferred parameters (error bars in Fig. 2) remains small, this reflects the strength of the fits and shows that the error is due to changes in the distribution functions not variability in fitting. The same

trend of increasing error as a function of super-Gaussian order is calculated for density. However, the error decreases or stays relatively constant as a function of the scattering parameter.

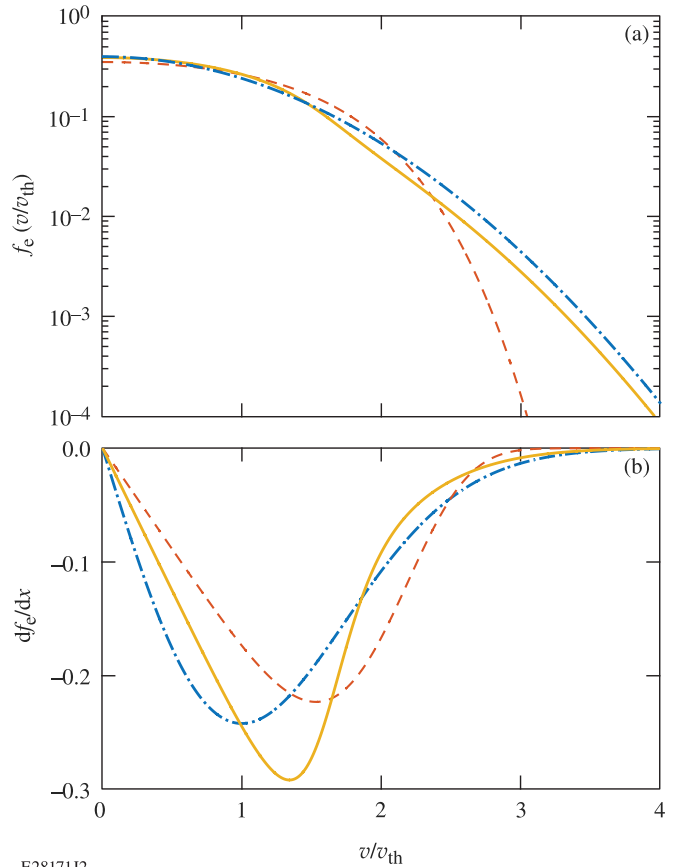


FIG. 3: Distribution function (a) and its derivative (b) with respect to x . A Maxwellian is shown in blue, while a super-Gaussian of order 5 is shown in red. A super-Gaussian of order 5 calculated when including Maxwellian tails (Eq. 8) is shown in orange.

The errors in the electron temperatures result from differences in the Maxwellian and non-Maxwellian electron distribution functions (Fig. 3) at velocities around the phase velocities of the electron plasma waves. Over the range of phase velocities studied ($\alpha \simeq 2 \rightarrow 4$), the super-Gaussian distributions have fewer electrons and a smaller slope than the Maxwellian electron distribution functions. This consequently reduces the Landau damping of the probed fluctuations, resulting in narrower peaks in the synthetic Thomson-scattering spectra. To compensate for the narrower peaks, the spectra calculated with the Maxwellian electron distribution functions (fits) have a reduced temperature (i.e. smaller Landau damping) than was used to generate the synthetic spectrum. The reduced electron temperature requires an increased electron density to maintain the resonant (peak) location of the electron plasma wave features. These trade-offs are illustrated in the Bohm-Gross dispersion relation,

$$\omega^2 = \omega_{pe}^2 + 3k^2 v_{th}^2.$$

As the phase velocities move farther into the tail of the electron distribution function, Landau damping decreases faster in the non-Maxwellian than in the Maxwellian calculations. This results in increased error as a function of phase velocity and super-Gaussian order, eventually leveling off as the damping rate in all cases approaches zero. The downward trend in density error with increasing phase velocity is also due to this apparent temperature. As the electron temperature decreases, a smaller change in electron density is required to maintain the resonant (peak) location of the electron plasma wave features.

These errors of 50% in temperature and 30% in density are for extreme changes to the electron distribution function, but even for small changes in the shape of the distribution function, the errors in temperature and density are larger than the statistical uncertainty of $\sim 5\%$ that is typical^{17,18} and can be a limiting factor in determining plasma conditions.

B. Super-Gaussians with Maxwellian tails

Both Fourkal et al.²³ and Brunner et al.²⁷ have proposed that the distribution function is super-Gaussian only at small velocities and trends toward Maxwellian at large velocities. These distribution functions could arise from a small anisotropy or nonlocal transport of electrons. The impact of this modified distribution function was investigated by altering Eq. (4) to include a super-Gaussian order that depends on velocity,²³

$$m \rightarrow m(x) = 2 + \frac{m-2}{1+(x/x^*)^9} \quad (8)$$

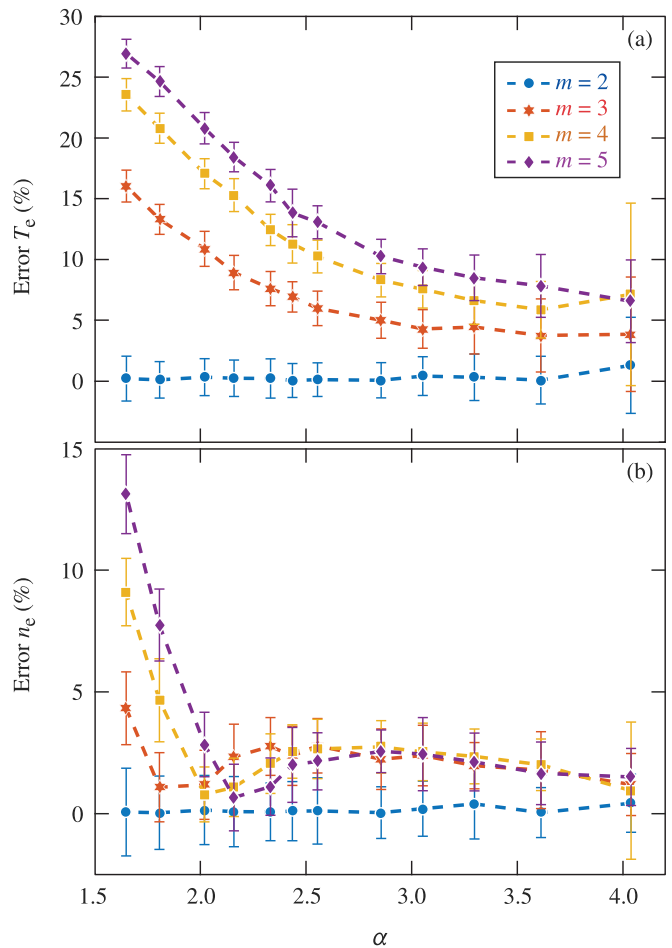
$$x_0 \rightarrow x_0[m(x)] \quad (9)$$

where

$$x^* = Z^{\frac{1}{2(m-1)}} \left[\frac{3\Gamma(3/m)}{\Gamma(5/m)} \right]^{\frac{m}{4(m-1)}} \quad (10)$$

In this form, the electron distribution function is unchanged for $x \ll x^*$ and becomes Maxwellian when $x \gg x^*$.

Figure 4 repeats the analysis shown in Fig. 2, but includes the modified non-Maxwellian electron distribution functions. The errors are reduced in this case, but when the phase velocities are small, errors of up to 30% in temperature and 13% in density are found. The trend in error with super-Gaussian order is preserved, but the trend with phase velocity is reversed. Density errors still show the trend of increased error with super-Gaussian order, but the error rapidly decreases with increasing phase velocity until $\alpha \simeq 2$, where the error effectively drops to zero.



E28026J1

FIG. 4: Percent error in (a) temperature and (b) density as a function of normalized phase velocity when the synthetic data generated by super-Gaussian electron distribution functions with Maxwellian tails (Eq. 8) are fit with spectrum that assume Maxwellian electron distribution functions. The values for 4 different super-Gaussian orders with Maxwellian tails are plotted in different colors with error bars that represent the standard deviation of 100 fits.

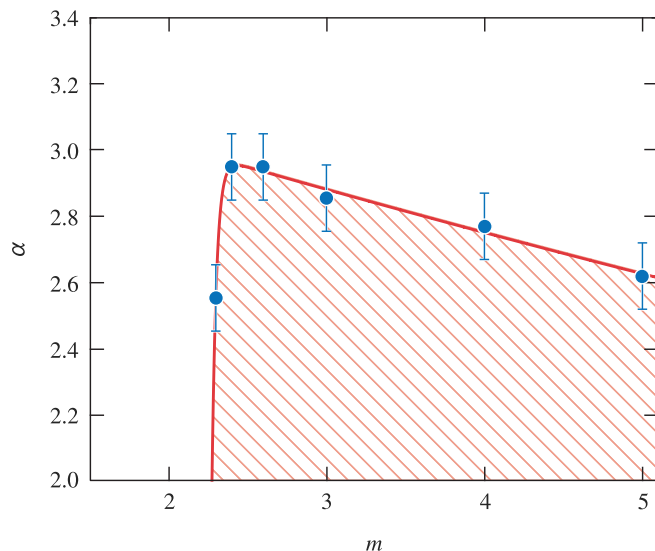
The trends in error are again due to deviations of the true distribution functions from a Maxwellian electron distribution function. For the calculations presented in Fig. 4, the effective ionization state (Z) was taken to be 1. This results in a small range for $x^* \simeq 1.57 \rightarrow 1.60$ when $m = 3 \rightarrow 5$. The reduction in errors calculated when including Maxwellian tails (Eq. 8) is a result of a convergence between the Maxwellian and non-Maxwellian electron distribution functions around the phase velocity of the electron plasma wave. In the case where the distribution function has Maxwellian tails, decreasing super-Gaussian order or increasing phase velocities results in less local deviation from a Maxwellian electron distribution function, at the phase velocity of the probed fluctuations. Therefore, the resonant frequency

and width of the electron plasma wave features are closer to the expected quantities, reducing the inferred errors. This trend sheds light on what might happen for arbitrary electron distribution functions: the greater the deviation from Maxwellian, especially in slope, the greater the possibility for error in inferred plasma conditions.

Figs. 2 and 4 illustrate a limited range of phase velocities. For smaller phase velocities, the distribution function has such a strong effect on the scattered spectra that it is not possible to reproduce key features of the Thomson-scattered spectra with a Maxwellian model. For larger phase velocities, the chosen spectral resolution (2 nm/resolution element) is on the order of the width of the peak.

The two cases presented, Figs. 2 and 4, represent the limiting cases for the effects of adding Maxwellian tails to the super-Gaussian electron distribution functions. As the ionization state is increased, the errors will transition from those presented in Fig. 4 to those presented in Fig. 2. However, it is worth noting that this is the result only for this formulation of super-Gaussian electron distribution functions with Maxwellian tails, and previous work^{20,24} has shown good agreement with a purely super-Gaussian distribution function.

C. Utilization of the complete high-frequency spectrum



E2802712

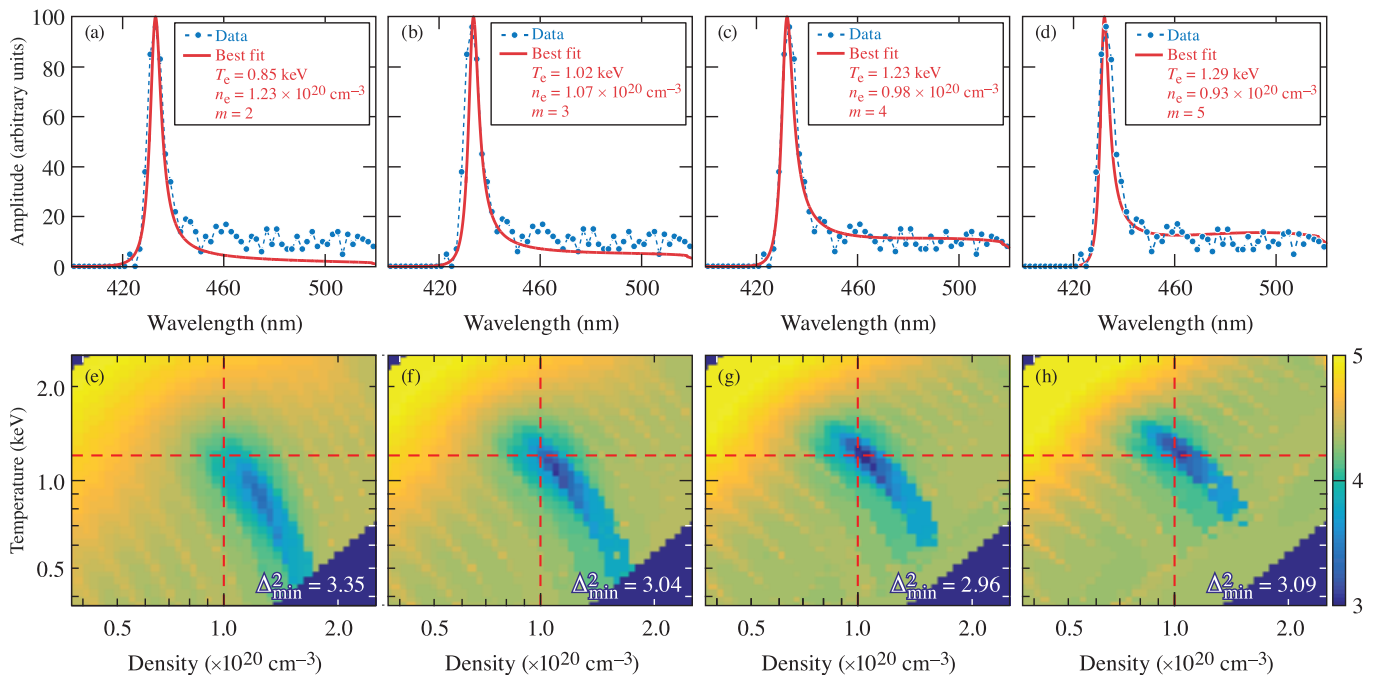
FIG. 5: Region where fits to the Stokes and anti-Stokes peaks yield different plasma conditions as a function of the super-Gaussian order. Error bars represent the uncertainty due to simulation resolution. Within the shaded region, different plasma conditions (namely electron temperature) are determined by fitting to synthetic Stokes and anti-Stokes shifted spectra, with a model that assumes a Maxwellian electron distribution function.

It is common to infer plasma parameters from a single electron plasma feature.¹⁷ In laser-produced plasmas there can be significant light scattered by other means at frequencies near one of the electron plasma wave resonances,²⁸ reducing the signal-to-noise ratio of the feature. However, in conditions where both electron plasma wave features can be measured, the Thomson-scattered spectrum provides more information about the shape of the distribution function. Figure 5 shows the conditions at which fits, that assume a Maxwellian electron distribution function, to the Stokes and anti-Stokes electron plasma wave features yield different plasma conditions (red shaded region). The data was generated as in Section III A. with the synthetic data created with a super-Gaussian electron distribution function. The Stokes and anti-Stokes shifted electron-plasma wave features were fit independently, and determined to yield the same plasma conditions when the temperature was in agreement to one standard deviation of 100 fits. Here, temperature was used because inferred density was found to be nearly the same between the two fits. Below the points, the two fits yield different temperatures. This indicates missing physics from the fit model; it is therefore possible to identify the distribution function as non-Maxwellian, but without further analysis it is not possible to identify the shape of the distribution function. Above the points, both fits yield the same plasma conditions but with the errors discussed in the previous sections.

The behavior in Fig. 5 is due to the competition between super-Gaussian order and the impact of the spectral resolution on the inferred temperature. For large super-Gaussian order the two peaks give the same temperature once the damping becomes so small that the width of the peaks are not resolved by the instrument. This leads to a decrease in the boundary, α , with super-Gaussian order, as increasing the super-Gaussian order decreases the damping on the wave (Fig. 3). When the super-Gaussian order is small, it becomes impossible to see the difference in the damping between the two peaks because the change in the damping, along with the resulting inferred temperature, falls below the precision of the measurement due to the imposed limited spectral resolution. Because this curve is highly dependent on spectral resolution, only the overall trend is meaningful.

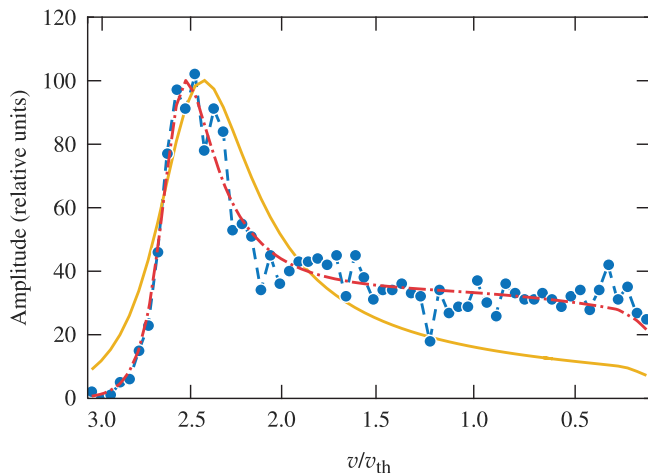
IV. NON-MAXWELLIAN ANALYSIS

Figure 6 shows that a global minimum in the fit metric can be found by changing the super-Gaussian order in the analysis. There is a well-defined minimum in the fit metric when data generated with $m = 4$ (Eq. 4) is fit with $m = 2$ [Fig. 6 (a, e)]. However, the fit metric gets smaller as the super-Gaussian order goes to the correct value (third column). This improvement is due to the shape of the spectrum not just the width and peak location, which can be seen in the top images [Fig. 6 (a, b, c, d)]. As the super-Gaussian order goes to the correct



E28028J2

FIG. 6: Images of the fit-metric as a function of temperature and density at $m = 2, 3, 4,$ and 5 . The value of the fit metric is shown on a logarithmic scale with the smallest value representing the “best” fit. Each image of the fit-metric space is paired with a lineout of the data and the fit that corresponds to the minimum in the fit space. The data was generated with electron density 10^{20} electrons/cm 3 , temperature of 1.2 keV, and $m = 4.0$ ($\alpha = 2.33$).



E28029J1

FIG. 7: Synthetic scattered spectrum for electron density 10^{20} electrons/cm 3 , temperature of 2 keV, and $m = 5.0$. A fit to the data using a non-Maxwellian model (red) and a fit using the standard Maxwellian model (yellow) are shown.

solution ($m = 4$), the slope on the small wavelength side of the peak steepens to match the data and the flatter region on the longer wavelength side rises to match the data. Additionally, the images on the bottom show the location of the minimum shifting toward the true values.

Figure 6 provides insight into the error bars in Figs. 2 and 4. Multiple local minima can be seen for each super-Gaussian order in Fig. 6. While none of the local minima in Fig. 6 are low enough for the gradient decent minimizer to stop, this is not the case at other scattering parameters. The multiple minima increase the uncertainty of the fit and correspondingly increase the error-bars. This effect occurs when the spectral feature becomes smaller than 3 resolution elements.

Allowing the distribution function, via super-Gaussian order, to change as a parameter in the fitting routine can eliminate model-dependent errors with minimally increased statistical uncertainty. Generally, when the super-Gaussian order of the distribution function is allowed to change, errors fall below 10%. There is a corresponding increase in the uncertainties due to the added fit parameter, and uncertainties go from a few percent to $\sim 10\%$. This is also the case for the distribution functions with Maxwellian tails described in Sec. III B, and it does not matter if one or both electron plasma wave features are used.

Figure 7 shows that including the true distribution function in the available fit space allows for elements of the synthetic spectrum to be reproduced that were not possible using Maxwellian analysis. The Maxwellian analysis is not capable of achieving the correct peak width or slope around $v/v_{th} = 2.5$. Maxwellian analysis under predicts the signal in the range from $0 < v/v_{th} < 1.5$. When super-Gaussian order is added as a fit

parameter, it becomes possible to match these spectral features for smaller phase velocities where they become more prominent. This is the case in Fig. 7 where $\alpha = 1.8$ putting it to the left of the data in Fig. 2.

V. SUMMARY

Assuming Maxwellian electron distribution functions in Thomson-scattering analysis was shown to produce significant errors in the inferred plasma temperature and density. Including the correct distribution function in accessible fit space, as done here with super-Gaussian order, can eliminate model-dependent errors with minimally increased statistical uncertainty. Including a super-Gaussian distribution function specifically can account for extra signal in the region between the electron plasma wave peaks. While not considered here, other distribution functions can correct other common problems in collective Thomson-scattering analysis such as peak signal asymmetry,⁷ relativistic effects,²⁹ and apparent shift in fundamental frequency required to fit both peaks simultaneously. This work shows the sensitivity of the collective Thomson spectrum to the shape of the underlying electron distribution function and suggests that collective Thomson scattering could be used to measure the complete electron distribution function.

VI. ACKNOWLEDGEMENT

This material is based upon work supported by the Department of Energy National Nuclear Security Administration under Award Number DE-NA0003856, the University of Rochester, and the New York State Energy Research and Development Authority.

This report was prepared as an account of work sponsored by an agency of the U.S. Government. Neither the U.S. Government nor any agency thereof, nor any of their employees, makes any warranty, express or implied, or assumes any legal liability or responsibility for the accuracy, completeness, or usefulness of any information, apparatus, product, or process disclosed, or represents that its use would not infringe privately owned rights. Reference herein to any specific commercial product, process, or service by trade name, trademark, manufacturer, or otherwise does not necessarily constitute or imply its endorsement, recommendation, or favoring by the U.S. Government or any agency thereof. The views and opinions of authors expressed herein do not necessarily state or reflect those of the U.S. Government or any agency thereof.

¹D. H. Froula, S. H. Glenzer, N. C. Luhmann, Jr., and J. Sheffield, *Plasma Scattering of Electromagnetic Radiation: Theory and Measurement Techniques*, 2nd ed. (Academic Press, Amsterdam, 2011).

²D. Turnbull, C. Goyon, G. E. Kemp, B. B. Pollock, D. Mariscal, L. Divol, J. S. Ross, S. Patankar, J. D. Moody, and P. Michel, *Phys. Rev. Lett.* **118**, 015001 (2017).

³C. Rousseaux, L. Gremillet, M. Casanova, P. Loiseau, M. Rabec Le Gloahec, S. D. Baton, F. Amiranoff, J. C. Adam, and A. Héron, *Phys. Rev. Lett.* **97**, 015001 (2006).

⁴D. S. Montgomery, R. P. Johnson, J. A. Cobble, J. C. Fernandez, E. L. Lindman, H. a. Rose, and K. G. Estabrook, *Laser Part. Beams* **17**, 349 (1999).

⁵S. Depierreux, C. Labaune, J. Fuchs, D. Pesme, V. T. Tikhonchuk, and H. A. Baldis, *Phys. Rev. Lett.* **89**, 045001 (2002).

⁶J. L. Kline, D. S. Montgomery, B. Bezzerides, J. A. Cobble, D. F. Dubois, R. P. Johnson, H. A. Rose, L. Yin, and H. X. Vu, *Phys. Rev. Lett.* **94**, 175003 (2005).

⁷R. J. Henchen, M. Sherlock, W. Rozmus, J. Katz, D. Cao, J. P. Palastro, and D. H. Froula, *Phys. Rev. Lett.* **121**, 125001 (2018).

⁸D. R. Gray and J. D. Kilkenny, *Plasma Phys.* **22**, 81 (1980).

⁹S. H. Glenzer, W. E. Alley, K. G. Estabrook, J. S. De Groot, M. G. Haines, J. H. Hammer, J. P. Jadaud, B. J. MacGowan, J. D. Moody, W. Rozmus, L. J. Suter, T. L. Weiland, and E. A. Williams, *Phys. Plasmas* **6**, 2117 (1999).

¹⁰D. H. Froula, J. S. Ross, L. Divol, N. Meezan, A. J. MacKinnon, R. Wallace, and S. H. Glenzer, *Phys. Plasmas* **13**, 052704 (2006).

¹¹C. A. Haynam, P. J. Wegner, J. M. Auerbach, M. W. Bowers, S. N. Dixit, G. V. Erbert, G. M. Heestand, M. A. Henesian, M. R. Hermann, K. S. Jancaitis, K. R. Manes, C. D. Marshall, N. C. Mehta, J. Menapace, E. Moses, J. R. Murray, M. C. Nostrand, C. D. Orth, R. Patterson, R. A. Sacks, M. J. Shaw, M. Spaeth, S. B. Sutton, W. H. Williams, C. C. Widmayer, R. K. White, S. T. Yang, and B. M. Van Wouterghem, *Appl. Opt.* **46**, 3276 (2007).

¹²J. L. Miquel, C. Lion, and P. Vivini, "The Laser Mega-Joule : LMJ & PETAL status and Program Overview," *J. Phys.: Conf. Ser.* **688**, 012067 (2016).

¹³W. Zheng, X. Wei, Q. Zhu, F. Jing, D. Hu, J. Su, K. Zheng, X. Yuan, H. Zhou, W. Dai, W. Zhou, F. Wang, D. Xu, X. Xie, B. Feng, Z. Peng, L. Guo, Y. Chen, X. Zhang, L. Liu, D. Lin, Z. Dang, Y. Xiang, and X. Deng, *High Power Laser Sci. Eng.* **4**, e21 (2016).

¹⁴O. L. Landen and R. J. Winfield, *Phys. Rev. Lett.* **54**, 1660 (1985).

¹⁵E. E. Salpeter, *Phys. Rev.* **120**, 1528 (1960).

¹⁶J. S. Ross, S. H. Glenzer, J. P. Palastro, B. B. Pollock, D. Price, L. Divol, G. R. Tynan, and D. H. Froula, *Phys. Rev. Lett.* **104**, 1528 (2010).

¹⁷J. S. Ross, S. H. Glenzer, J. P. Palastro, B. B. Pollock, D. Price, G. R. Tynan, and D. H. Froula, *Rev. Sci. Instrum.* **81**, 10D523 (2010).

¹⁸S. C. Snyder, L. D. Reynolds, J. R. Fincke, G. D. Lassahn, J. D. Grady, and T. E. Repetti, *Phys. Rev. E* **50**, 519 (1994).

¹⁹S. H. Glenzer, W. Rozmus, B. J. MacGowan, K. G. Estabrook, J. D. de Groot, G. B. Zimmerman, H. A. Baldis, J. A. Harte, R. W. Lee, E. A. Williams, and B. G. Wilson, *Phys. Rev. Lett.* **82**, 97 (1999).

²⁰J. Zheng, C. X. Yu, and Z. J. Zheng, *Phys. Plasmas* **4**, 2736 (1997).

²¹J. P. Matte, M. Lamoureux, C. Moller, R. Y. Yin, J. Delettrez, J. Virmont, and T. W. Johnston, *Plasma Phys. Control. Fusion* **30**, 1665 (1988).

²²A. B. Langdon, *Phys. Rev. Lett.* **44**, 575 (1980).

²³E. Fourkal, V. Y. Bychenkov, W. Rozmus, R. Sydora, C. Kirkby, and C. E. Capjack, *Phys. Plasmas* **8**, 550 (2001).

²⁴J. M. Liu, J. S. De Groot, J. P. Matte, T. W. Johnston, and R. P. Drake, *Phys. Rev. Lett.* **72**, 2717 (1994).

²⁵J. Katz, R. Boni, C. Sorce, R. Follett, M. J. Shoup III, and D. H. Froula, *Rev. Sci. Instrum.* **83**, 10E349 (2012).

²⁶fmincon Function, MATLAB® R2015b, The MathWorks Inc., Natick, MA 01760-2098, (<https://www.mathworks.com/help/optim/ug/fmincon.html>), 13 December 2018.

²⁷S. Brunner and E. Valeo, *Phys. Plasmas* **9**, 923 (2002).

²⁸G. F. Swadling, J. S. Ross, P. Datte, J. Moody, L. Divol,

O. Jones, and O. Landen, *Rev. Sci. Instrum.* **87**, 11D603 (2016).
²⁹J. P. Palastro, J. S. Ross, B. Pollock, L. Divol, D. H. Froula, and

S. H. Glenzer, *Phys. Rev. E* **81**, 036411 (2010).